Journal of Cerebral Blood Flow & Metabolism (2015) 35, 1426–1434

www.jcbfm.com

ORIGINAL ARTICLE

Aberrant white matter networks mediate cognitive impairment in patients with silent lacunar infarcts in basal ganglia territory

Jinfu Tang[1,2,4], Suyu Zhong[1,4], Yaojing Chen[1,2,4], Kewei Chen[1,3], Junying Zhang[1,2], Gaolang Gong[1], Adam S Fleisher[3,5], Yong He[1] and Zhanjun Zhang[1,2]

Silent lacunar infarcts, which are present in over 20% of healthy elderly individuals, are associated with subtle deficits in cognitive functions. However, it remains largely unclear how these silent brain infarcts lead to cognitive deficits and even dementia. Here, we used diffusion tensor imaging tractography and graph theory to examine the topological organization of white matter networks in 27 patients with silent lacunar infarcts in the basal ganglia territory and 30 healthy controls. A whole-brain white matter network was constructed for each subject, where the graph nodes represented brain regions and the edges represented interregional white matter tracts. Compared with the controls, the patients exhibited a significant reduction in local efficiency and global efficiency. In addition, a total of eighteen brain regions showed significantly reduced nodal efficiency in patients. Intriguingly, nodal efficiency–behavior associations were significantly different between the two groups. The present findings provide new aspects into our understanding of silent infarcts that even small lesions in subcortical brain regions may affect large-scale cortical white matter network, as such may be the link between subcortical silent infarcts and the associated cognitive impairments. Our findings highlight the need for network-level neuroimaging assessment and more medical care for individuals with silent subcortical infarcts.

Journal of Cerebral Blood Flow & Metabolism (2015) **35,** 1426–1434; doi:10.1038/jcbfm.2015.67; published online 15 April 2015

Keywords: connectome; diffusion tensor imaging; graph theory; silent lacunar infarcts; white matter network

INTRODUCTION

Silent lacunar infarcts are observed in over 20% of healthy elderly individuals, and their prevalence and size increase with age.[1] Although silent lacunar infarcts lack clinical stroke-like symptoms, they are associated with subtle deficits in physical and cognitive functions, which are indicated by defects in perceptual speed, semantics, and episodic memory.[2] Significant link has been observed between silent lacunar infarcts in both cortical and subcortical regions and the risk of subsequent stroke and dementia.[1] In recent findings, disrupted white matter has been suggested to mediate the relationship between multiple small vessel diseases including cerebral microbleeds in early Alzheimer's disease (AD),[3] lacunar infarcts,[4] cerebral amyloid angiopathy,[5] and cognitive dysfunction. However, it remains unclear whether disrupted white matter (WM) contributes to the neural mechanism by which silent subcortical lacunar infarcts lead to cognitive impairment.

The human brain is a well-organized network, performing rapid information processing. Recent progress in advanced neuroimaging techniques, together with well-developed analytical procedures such as graph theory, makes it possible to noninvasively map large-scale patterns of structural and functional connectivity in the human brain (referred to as the human connectome)[6] and to characterize the topological properties of brain networks in the context of health and disease.[7] Several studies have examined the topological organization of whole-brain structural and functional networks in lacunar-infarct-related brain diseases, such as stroke,[8] mild cognitive impairment (MCI),[9,10] and AD,[10–13] finding disrupted integration of the system. However, it is largely unknown whether and how subcortical brain regions disrupt the topological properties of whole-brain networks.

Multiple basal ganglia–cortical loops are believed to be involved in motivational and cognitive components of behavior, including reward-based reversal learning,[14] visuomotor and cognitive procedural learning in children,[15] and working memory.[16] Thus, it is important to investigate the basal ganglia–cortical loop-related networks in a group with lacunar infarcts in the basal ganglia territory. Studying this issue will provide crucial insights into how subcortical lesions result in cognitive decline.

We hypothesized that silent lacunar infarcts in the basal ganglia territory could be related to abnormal topological organization of the whole brain and may account for the observed cognitive decline. In the present study, diffusion tensor imaging (DTI)-based structural network analysis was utilized to examine the differences

[1]State Key Laboratory of Cognitive Neuroscience and Learning, Beijing Normal University, Beijing, China; [2]BABRI Centre, Beijing Normal University, Beijing, China and [3]Banner Alzheimer's Institute, Phoenix, Arizona, USA. Correspondence: Dr Z Zhang, State Key Laboratory of Cognitive Neuroscience and Learning, Beijing Normal University, Beijing 100875, China.
E-mail: zhang_rzs@bnu.edu.cn
This study was supported by The State Key Program of National Natural Science of China (Grant No.81430100), Beijing New Medical Discipline Based group (Grant No.100270569); the Natural Science Foundation of China (Grant No. 30873458 and 81173460); and the State Key Program of National Natural Science of China (Grant No. 81430100); project of Institute of Basic Research in Clinical Medicine, China Academy of Chinese Medical Sciences (Grant No. Z0251 and No.Z0288), program for New Century Excellent Talents in University (Grant No. NCET-10-0249), and National Science Fund for Distinguished Young Scholars (Grant No. 81225012).
[4]These authors contributed equally to this work.
[5]Current address: Eli Lilly and Co, Indianapolis, IN, USA.
Received 20 November 2014; revised 16 February 2015; accepted 16 March 2015; published online 15 April 2015

of topological organization of the cortical white matter structural network in patients with silent lacunar infarcts (LACI) in the basal ganglia, compared with healthy controls (HCs). We also investigated the association of network topological properties with neuropsychological performance in both the groups. This study provides a detailed understanding of whether and how the presence/absence of subcortical silent lacunar infarction affects cortical WM network that may account for cognitive decline.

MATERIALS AND METHODS

Participants

The subjects included in our study were from the BABRI (Beijing Aging Brain Rejuvenation Initiative) database. The BABRI is a large, longitudinal aging project with the aim of collecting data on cognitive, behavioral, and social-demographic factors, together with other potentially influential factors, and necessary clinical data for 1,600 Beijing elder citizens at five time points over 10 years.

Subjects' inclusion in the BABRI study was predicated on their age ($\geqslant$50 years old), education status (no less than 6 years of education), and their consent to participate voluntarily. We also acquired magnetic resonance imaging (MRI) data for a subset of the BABRI participants who were willing to participate in this additional imaging procedure and met its physical demands. Of the 1,600 individuals in the first time-window of the BABRI study, 202 participants underwent imaging, including 56 patients with mild cognitive impairments, 25 patients with stroke (size of the ischemic infarction >15 mm), 41 patients with a history of diabetes, and 80 participants in the current study.

To be included in this study, participants had to meet the following three additional criteria: (1) a score of at least 24 on the Mini-Mental Status Examination (MMSE); (2) no history of coronary disease, diabetes, nephritis, tumors, gastrointestinal disease, or psychiatric illness; and (3) no history of use of psychoactive medications. A total of 80 participants met these criteria, including 39 patients with LACI and 41 HCs. Of the 39 patients with LACI, 9 patients were excluded because of temporal, frontal, or brain stem infarcts on their MRIs, and another 3 were excluded because of poor image quality. Of the 41 HC subjects, 11 were excluded because of dropout during MRI scan ($n=4$), poor image quality ($n=2$), or existence of suspected ischemic infarction with size <3 mm ($n=5$). The present analyses included 27 LACI patients and 30 controls. In the present study, we recruited elderly subjects from communities, which could decrease the bias of clinical referral study, which tended to recruit more severe impairment patients. Considering the combined effects of white matter lesions and small deep infarcts, we only include the pure lacunar infarcts patients in the present study. The study protocol was approved by the Institutional Review Board of Beijing Normal University Imaging Center for Brain Research and the study was performed according to the ethical principles of the Declaration of Helsinki. Written consent form was obtained from each subject.

The participants' medical history and scans were separately reviewed by two experienced neurologists. The lacunar infarcts were determined by visual inspection of the T1-, T2-FLAIR, and T2-weighted sequences of MRI scans. Our judgment is based on STRIVE criteria[17] and Fisher criteria.[18] We defined lacunar infarcts as round or ovoid lesions of increased signal relative to white matter on T2WI and T2-FLAIR images, or decreased attenuation similar to cerebrospinal fluid-filled cavities on T1-weighted images, 3 to 15 mm in diameter.[18] All of the patients had lacunar infarcts in the basal ganglia territory, which included the caudate nucleus ($n=4$), putamen ($n=11$), globus pallidus ($n=2$), internal capsule ($n=12$), and thalamus ($n=7$), detailed locations are presented in Supplementary Table 1.

Neuropsychological Testing

All the participants received a battery of six categories of neuropsychological tests to assess general mental status and other cognitive domains, such as episodic memory, executive function, and language ability. All the neuropsychological tests followed our previous study.[19] General mental status was assessed using the Mini-Mental Status Examination. The comprehensive neuropsychological battery consisted of five cognition domains. The memory tests included the Auditory Verbal Learning Test (AVLT), Digit Span, and the Rey-Osterrieth Complex Figure test (ROCF). The participants underwent visual-spatial tests, which included the ROCF (copy) and the Clock-Drawing Test (CDT). The participants completed the Stroop Color and Word Test (SCWT)-A and the Symbol Digit Modalities Test (SDMT), which are measures of attention functions. Executive function was assessed with the SCWT-B and SCWT-C. Last, language ability was assessed with the Boston Naming Test and the Category Verbal Fluency Test. The neuropsychological characteristics for each group are presented in Table 1.

Magnetic Resonance Imaging Data Acquisition

The MRI data were acquired on a 3.0T Siemens Tim Trio MRI scanner in the Imaging Center for Brain Research, Beijing Normal University, and included one high-resolution T1 scan and two sets of diffusion magnetic resonance imaging data scans. T2-weighted and T2-FLAIR images were acquired for all the participants. A high-resolution T1-weighted image covering the whole brain was acquired using a sagittal three-dimensional magnetization prepared rapid gradient echo (MP-RAGE) sequence. The detailed scanning parameters were as follows: repetition time (TR) = 1,900 milliseconds; echo time (TE) = 3.44 milliseconds; inversion time (TI) = 900 milliseconds; slice thickness = 1 mm; no inter-slice gap; 176 axial slices; matrix size = 256×256; field of view = 256×256 mm^2; flip angle = 9°; voxel size = $1\times1\times1$ mm^3. For each diffusion MRI scan, diffusion images covering the whole brain were acquired by a single-shot echo planar imaging-based sequence with the following scan parameters: TR = 9,500 milliseconds; TE = 92 milliseconds; 30 diffusion-weighted directions with a b value of 1,000 seconds/mm^2, and a single image with a b value of 0 seconds/mm^2; slice thickness = 2 mm; no inter-slice gap; 70 axial slices; matrix size = 128×124; field of view = 256×248 mm^2; voxel size = $2\times2\times2$ mm^3.

Image Pre-Processing

All the image preprocessing and analyses described below were implemented using a pipeline tool for diffusion MRI (PANDA).[20] First, the skulls were stripped from the T1-weighted image and diffusion MRI for each participant. Each diffusion-weighted image was then co-registered to the b0 image using an affine transformation to correct the eddy-current-induced distortions and simple head-motion artifacts. The diffusion gradient directions were adjusted accordingly.[21] To obtain the brain size of each subject, the volume of the gray matter, WM, and cerebrospinal fluid were computed using the VBM8 toolbox[22] in SPM8 (www.fil.ion.ucl.ac.uk/spm/).

Diffusion Tensor Imaging-Based Structural Network Construction

In graph theory, a network comprises two fundamental elements: nodes and edges. Here, we constructed DTI-based structural brain networks at the macro-scale, where nodes represent brain regions and edges represent interregional white matter tracks. Figure 1 illustrates the flowchart of DTI-based brain network construction in this study.

White matter tractography. Deterministic tractography was performed to obtain whole-brain white matter tracts. Specifically, the fiber assignment continuous tracking (FACT) algorithm was applied to reconstruct whole-brain tracts.[23] To eliminate the impact of the seed point's number and position, a single seed point was positioned in the center of each voxel of the whole brain. A tract was terminated if the turn angle of the fiber was $>45°$ or the fiber entered a voxel with the fractional anisotropy <0.2. The tracking procedure was performed using the Diffusion toolkit (http://trackvis.org) that is embedded in PANDA.

Network node definition. The nodes were defined in native space for each individual using the procedure proposed by Gong *et al*.[24] Briefly, the skull-stripped T1-weighted image was non-linearly and spatially normalized to Montreal Neurological Institute space using FMRIB's Linear Image Registration Tool (FNIRT, FSL, http://www.fmrib.ox.ac.uk/fsl/). The individual fractional anisotropy images were co-registered to the individual skull-stripped T1-weighted images. To transform the automated anatomic labeling atlas from Montreal Neurological Institute space to DTI native space, the inverse transformations achieved in the above two steps were successively applied to the automated anatomic labeling atlas. As a result, the individual cerebrum in native space was divided into 90 regions corresponding to the AAL atlas (45 regions for each hemisphere, excluding the brain stem and cerebellum), including 78 cortical regions and 12 subcortical regions. Each region represents a node of the DTI-based structural brain network.

Network edge definition. The network edges were defined by the tracts derived from whole-brain tractography. Here, we focused on binary DTI-based structural networks given the difficulties in determining the

diffusion-based connectivity strength that is biologically meaningful. Two regions, A and B, were considered to be structurally connected if there existed at least one tract with terminal points occurring in regions A and B. We therefore obtained a symmetric 90×90 binary network matrix representing the existence or absence of a link between any two regions for each individual. In this study, we also assessed thresholding effects on

Table 1. Demographic and Neuropsychological test results for silent lacunar infarcts and healthy control groups

Tests	*LACI* (n = *27*)	*HC* (n = *30*)	T-*value* (X^2)	P-*value*
Gender	19M/8F	12M/18F	5.284[a]	0.033
Age (years)	65.81 ± 5.93	63.53 ± 6.11	1.428	0.159
Education (years)	11.96 ± 3.34	11.06 ± 3.11	1.047	0.299
Hypertension (%)	8 (29.6%)	6 (20%)	0.711[a]	0.540
Smoking				
Non/past/current	21/ 1/ 5	27/ 0/ 3	2.098[a]	0.177
General mental status				
MMSE	26.37 ± 2.45	27.93 ± 1.55	− 2.906	0.005
Memory				
AVLT-delay recall	3.48 ± 2.73	5.10 ± 2.01	− 2.564	0.013
AVLT-T	22.07 ± 9.68	29.17 ± 7.18	− 3.161	0.003
ROCF-delay recall	13.07 ± 8.87	13.20 ± 5.29	− 0.066	0.948
Digit Span	11.78 ± 2.29	11.70 ± 2.12	0.13	0.89
Spatial processing				
ROCF-Copy	32.41 ± 5.89	33.53 ± 2.62	− 0.949	0.347
CDT	24.33 ± 4.22	24.57 ± 3.78	− 0.220	0.827
Attention				
SCWT-A-Time	31.44 ± 9.15	28.00 ± 8.44	1.478	0.145
SDMT	30.44 ± 12.39	37.87 ± 9.55	− 2.547	0.014
Executive function				
SCWT-B-Time	45.70 ± 13.57	38.50 ± 9.48	2.342	0.023
SCWT-C-Time	86.00 ± 27.81	80.33 ± 28.18	0.763	0.449
SCWT-C-Right	43.56 ± 5.73	46.07 ± 2.52	− 2.178	0.034
Language ability				
BNT	23.96 ± 3.48	24.13 ± 3.53	− 0.183	0.855
CVFT	39.85 ± 9.89	45.70 ± 11.53	− 2.043	0.046

Abbreviations: AVLT, Auditory Verbal Learning Test; BNT, Boston Naming Test; CDT, Clock-Drawing Test; CVFT, Category Verbal Fluency Test; MMSE, Mini-Mental State Examination; ROCF, Rey-Osterrieth Complex Figure test; SCWT-A, -B, -C, Stroop Color and Word Test-A, -B, -C; SDMT, Symbol Digit Modalities Test. [a]The *P*-value for gender, hypertension, and smoking ratio in the two groups was obtained using a Chi-square test. Values are mean ± s.d. The comparisons of neuropsychological scores between the two groups were performed with independent two-sample *t*-tests. $P < 0.05$ was considered significant.

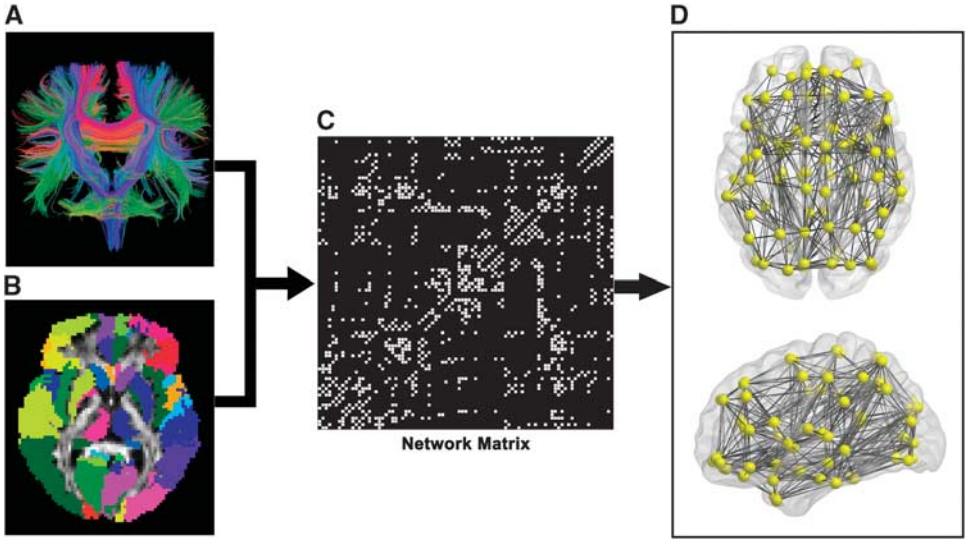

Figure 1. Flowchart for the construction of the DTI-based structural brain network. (**A**) White matter fibers reconstructed by deterministic tractography. (**B**) The subject-specific AAL mask in the DTI native space. Each color represents a node of the DTI brain network. (**C**) The binary network matrix. (**D**) The three-dimensional representation of the anatomic brain network. AAL, automated anatomic labeling; DTI, diffusion tensor imaging.

the results of the network analysis by applying thresholding with a different number of fibers, ranging from 1 to 5. The analysis showed our primary results remained nearly the same at different fiber number thresholds (Supplementary Table 2). In this study, we report our results based primarily on binary networks constructed by thresholding with one track.

Brain Network Analysis

Graph theoretical measures were used to characterize topological architectures of the DTI-based structural brain networks derived above. In the current study, we used network efficiency indices because of their power in characterizing the capacity of parallel information processing in both connected and disconnected networks.[25] Specifically, four indices (global efficiency, local efficiency, small-worldness, and nodal efficiency, see definitions below) were examined for each network in this study. The four indices were chosen because these indices showed abnormalities in previous report on lacunar infarct–related brain diseases, such as stroke[8] and AD.[10–13]

Global efficiency. Global efficiency is a global measure of the parallel information transfer ability in the whole network. It is computed as the average of the inverse of the 'harmonic mean' of the characteristic path length:[26]

$$E_{\text{glob}} = \frac{1}{N(N-1)} \sum_{i \neq j \in \text{G}} \frac{1}{L_{ij}}$$

where N is the number of nodes in the graph G, and L_{ij} is the characteristic path length between nodes i and j. The characteristic path length in a binary graph refers to the number of distinct edges along the shortest path between nodal pairs.

Local efficiency. Local efficiency quantifies the ability of a network to tolerate faults, corresponding to the efficiency of the information flow between the nearest neighbors of the node i. The local efficiency of a network is computed as follows:

$$E_{\text{loc}} = \frac{1}{N} \sum_{i \in \text{G}} E_{\text{glob}}(\text{G}_i)$$

where G_i is the sub-graph composed of the nearest neighbors of node i and the connections among them.

Small-worldness. The concept of small-worldness was originally proposed by Watts and Strogatz.[27] Specifically, a small-world network has highly local clustering (i.e., neighboring nodes are connected tightly) and short average paths (i.e., one node is only a few paths away from any other node in the network), thereby showing high efficiency of both segregated and integrated processing. The fundamental idea behind small-world networks is the notion that the networks gain efficiency by having a large number of local connections and very few global links connecting local clusters together. In this study, we used the procedure that Gong *et al*.[24] adopted to evaluate small-worldness. The random rewiring procedure depicted by Maslov and Sneppen[28] was used to yield 100 matched random networks for each subject, with the same number of nodes and edges and the same degree distribution as the real network. Typically, a small-world network should meet the following criteria: $E_{\text{loc}}(\text{G})/E_{\text{loc}}(G_{\text{random}}) > 1$, $E_{\text{glob}}(\text{G})/E_{\text{glob}}(\text{G}_{\text{random}}) \approx 1$, where G refers to the real brain network and G_{random} refers to the random network.

Nodal efficiency. Efficiency of a node is a measure of its capacity to communicate with other nodes of the network. The nodal efficiency for a given node (E_{nodal}) was defined as the inverse of the harmonic mean of the shortest path length between this node and all other nodes in the network.[25] The nodes with high nodal efficiency values can be categorized as hubs in a network. Nodal efficiency (E_{nodal}) was computed by the equation below:

$$E_{\text{nodal}}(i) = \frac{1}{N-1} \sum_{i \neq j \in \text{G}} \frac{1}{L_{ij}}$$

where L_{ij} is the shortest path length between node i and node j. Here, node i is considered to be a brain hub if $E_{\text{nodal}}(i)$ is at least 1 s.d. greater than the average nodal efficiency of the network.

Statistical Analysis

Two-sample *t*-tests were used to test between-group differences in age and brain size, while χ^2 tests were used to compare gender. For graph theoretical measures, general linear models were applied to determine between-group differences in the topological parameters (local efficiency, global efficiency, and nodal efficiency) of DTI-based structural brain networks. Age, gender, and brain size were included as covariates in the general linear models because these factors were found to be significantly correlated with the topological parameters of structural brain network.[29] Specifically, the general linear models are as follows: $Y = \beta_0 + \beta_1 \times \text{Group} + \beta_2 \times \text{Age} + \beta_3 \times \text{Gender} + \beta_4 \times \text{Brain Size}$, where Y is the topological parameter. The group difference was determined by examining the null hypothesis of $\beta_1 = 0$. We plotted the receiver-operating characteristic (ROC) curves to determine whether graph-based network metrics might serve as biomarkers for diagnosing LACI. For the nodal efficiency metric, we applied the false discovery rate procedure to correct the multiple comparisons at a q value of 0.05. In addition, for the network metrics showing significant between-group differences, we further used the following general linear models to test whether the relationships between network metrics (both global metrics and nodal efficiency) and cognitive performance differed between the two groups by examining the interaction term of Group × X: $Y = \beta_0 + \beta_1 \times \text{Group} + \beta_2 \times \text{X} + \beta_3 \times \text{Group} \times \text{X} + \beta_4 \times \text{Age} + \beta_5 \times \text{Gender} + \beta_6 \times \text{Brain Size}$, where Y is the cognitive performance and X is one of the three network efficiency indices. The interaction term was tested by examining the null hypothesis of $\beta_3 = 0$. This testing was implemented by analyzing the interaction effect in a linear mode that included the network metrics as dependent variables; group, behavior, and their interaction as independent variables; and age, gender, and brain size as covariates. A threshold value for establishing the significance of group effects was set at $P < 0.05$ (uncorrected for multiple comparisons).

Validation Analysis

To test the reproducibility of our findings, a repeated 'split-half' method was applied. Briefly, a subgroup was generated by randomly selecting half the subjects in the LACI group ($n = 14$) and the HC group ($n = 15$) after controlling for the effects of age, gender, and brain size. Next, a two-sample *t*-test was used to detect network efficiency differences between the selected subgroups. The procedure was repeated 100 times. For global and local efficiency, the number of subgroups showing parallel significant between-group differences with the whole group analysis (27 patients with LACI and 30 HCs) was computed. To determine the reproducibility of nodal efficiency, Pearson's correlation coefficients for nodal t values from each split-half subgroup and the whole group were computed.

To further test the reproducibility of our findings across DTI processing platforms, the image processing and network construction were re-run by using another DTI platform, DTI studio (H Jiang and S Mori, The Johns Hopkins University, Baltimore, MD, USA), and the same statistical analysis was re-applied.

RESULTS

Demographics and Neuropsychological Testing

No significant differences were observed for age or years of education between the HCs and the patients with LACI ($P > 0.05$). There were no significant group differences in smoking habits ($\chi^2 = 2.27$, $P = 0.15$) or medical history of hypertension ($\chi^2 = 0.71$, $P = 0.54$). In the patients, cognitive function in the domains of general mental status, memory, attention, executive function, and language ability were significantly worse than for HCs, but no differences in spatial processing ability were observed. The demographic and neuropsychological testing data are presented in Table 1.

Global Topological Organization of the Diffusion Tensor Imaging-Based Network

Both the patients and the controls exhibited economical small-world organization for the constructed networks. Specifically, compared with a matched random network, the DTI-based brain networks had slightly decreased global efficiency but much higher local efficiency (Supplementary Figure 1). Nevertheless, quantitative statistical analyses indicated significant reductions in both

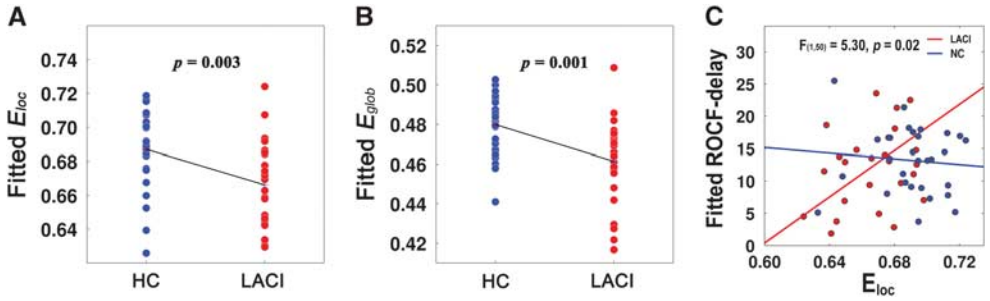

Figure 2. Between-group differences in global properties and the correlation between global properties and cognitive performances. HC, healthy control (blue). LACI, silent lacunar Infarction in basal ganglia (red). In global properties, the LACI group had significantly decreased local efficiency (E_{loc}, **A**) and global efficiency (E_{glob}, **B**) in DTI-based brain networks compared with the HC group. The correlation between local efficiency and ROCF-delay recall (**C**) showed a significant group difference ($F_{1,50} = 5.30$, $P = 0.025$, **C**). Note that all results were obtained using a general linear model to control for the effects of age, gender, and brain size. DTI, diffusion tensor imaging; ROCF, Rey-Osterrieth Complex Figure test.

Table 2. Brain regions showing significant group differences in the nodal efficiency between silent lacunar infarcts and healthy control groups

Regions	E_{nodal} *in LACI (Mean ± s.d.)*	E_{nodal} *in HC (Mean ± s.d.)*	*Group effect*	
			T-*value*	*Corrected* P-*value*
ORB_{inf}.L	0.465 ± 0.039	0.510 ± 0.034	−4.304	0.000074
PCUN.L	0.553 ± 0.030	0.599 ± 0.042	−3.881	0.000295
PHG.L	0.445 ± 0.026	0.473 ± 0.018	−3.815	0.000363
SFG_{med}.L	0.463 ± 0.040	0.502 ± 0.032	−3.745	0.000452
PoCG.R	0.465 ± 0.030	0.498 ± 0.034	−3.572	0.000773
PCL.R	0.431 ± 0.034	0.467 ± 0.028	−3.503	0.000955
IFG_{triang}.L	0.451 ± 0.040	0.502 ± 0.055	−3.351	0.001506
MFG.L	0.398 ± 0.031	0.430 ± 0.033	−3.321	0.001646
SOG.R	0.503 ± 0.044	0.539 ± 0.032	−3.167	0.002575
PCL.L	0.453 ± 0.030	0.483 ± 0.029	−2.885	0.005683
SPG.R	0.475 ± 0.041	0.509 ± 0.037	−2.832	0.006567
ORB_{supmed}.L	0.448 ± 0.037	0.467 ± 0.024	−2.819	0.006803
ORB_{sup}.R	0.478 ± 0.043	0.507 ± 0.038	−2.791	0.007324
PCUN.R	0.557 ± 0.037	0.582 ± 0.030	−2.719	0.008880
IFG_{triang}.R	0.442 ± 0.055	0.485 ± 0.050	−2.700	0.009345
ITG.L	0.456 ± 0.045	0.482 ± 0.033	−2.682	0.009795
DCG.L	0.461 ± 0.031	0.482 ± 0.016	−2.681	0.009810
DCG.R	0.458 ± 0.035	0.487 ± 0.031	−2.659	0.010389

Abbreviations: DCG, median cingulate and paracingulate gyri; HC, healthy control; IFG_{triang}, triangular part of the inferior frontal gyrus; ITG, inferior temporal gyrus; LACI, silent lacunar infarcts; MFG, middle frontal gyrus; ORB_{inf}, orbital part of inferior frontal gyrus; ORB_{sup}, orbital part of the superior frontal gyrus; ORB_{supmed}, medial orbital portions of superior frontal gyrus; PCL, paracentral lobule; PCUN, precuneus; PHG, parahippocampal gyrus; PoCG, postcentral gyrus; SFG_{med}, medial superior frontal gyrus; SOG, superior occipital gyrus; SPG, superior parietal gyrus. The binary diffusion tensor imaging (DTI)-based network for each participant was constructed using an automated anatomic labeling template. The comparison of nodal efficiency was performed between two groups (LACI and HC groups) using general linear model. The age, gender, and brain size effects were removed in group comparison analyses. For comparison of the 90 brain regions, $q < 0.05$ (corrected) was considered significant. For *T* values, negative value represents LACI < HC.

local efficiency ($P = 0.003$; HC: 0.69 ± 0.02; LACI: 0.67 ± 0.03) and global efficiency ($P = 0.001$; HC: 0.48 ± 0.02; LACI: 0.46 ± 0.02) in patients with LACI (Figure 2). These results remained unchanged when networks were constructed using different fiber number thresholds (Supplementary Materials, Table 2).

Nodal Topological Organization of the Diffusion Tensor Imaging-Based Network

The distribution of hub nodes identified by E_{nodal} in the HC and LACI groups are shown in Figure 3. Ten same hub regions were identified in both groups, including the bilateral precuneus (PCUN), bilateral calcarine (CAL), bilateral caudate (CAU), bilateral putamen (PUT), right superior occipital gyrus (SOG), and left thalamus (THA), and one hub region, the left SOG, was identified as a hub only in the HC group (Figure 3). However, 18 brain regions exhibited significantly reduced nodal efficiency ($q < 0.05$, false discovery rate corrected) in the patients with LACI, including 11 cortical association regions (the left middle frontal gyrus (MFG), the bilateral triangular part of the inferior frontal gyrus (IFG_{triang}), the left medial superior frontal gyrus (SFG_{med}), the right SOG, right superior parietal gyrus (SPG), bilateral PCUN, the bilateral paracentral lobule (PCL), and the left inferior temporal gyrus (ITG)), six paralimbic regions (the right orbital part of the superior frontal gyrus (ORB_{sup}), the left orbital part of inferior frontal gyrus (ORB_{inf}), the left medial orbital portions of superior frontal gyrus (ORB_{supmed}), the bilateral median cingulate and paracingulate gyri (DCG), and the left parahippocampal gyrus (PHG)), and one primary cortical region (the right postcentral gyrus (PoCG)), as shown in Figure 3 and Table 2. Among the 18 regions, 10 (55.5% of 18) were located in the left hemisphere and 8 regions (44.5% of 18) were in the right hemisphere.

Group Effects on Correlations Between Network Properties and Cognitive Performance

For the global measures, statistical analysis revealed significant group differences in the correlation between local efficiency and ROCF-delay recall ($F_{1,50} = 5.30$, $P = 0.025$, Figure 2C). The R^2 values for the correlations between local efficiency and ROCF delay for the LACI and HC groups were 0.1494 and 0.0177, respectively. But there were no group differences in the correlation between global efficiency and any cognitive measures.

In addition to the global measures, group differences in the correlation between nodal efficiency and cognitive performance were also examined. It is important to note that we only considered regions exhibiting significant group differences in nodal efficiency in subsequent brain-behavior correlation studies. Eleven correlations between nodal efficiency and cognitive measures showed significant differences between the groups ($P < 0.05$), including IFG_{triang}.L with AVLT-T; ITG.L with SCWT-A-Time; PCL.R with AVLT-T, AVLT-delay-recall, SDMT, SCWT-A-Time, and Category Verbal Fluency Test; PCL.L with ROCF-Copy and CDT; SFG_{med}.L with CDT; PHG.L with CDT. These results are shown in Table 3 and Figure 4. Notably, the significant correlation results were not corrected for multiple comparisons and, therefore, should be regarded as exploratory in nature.

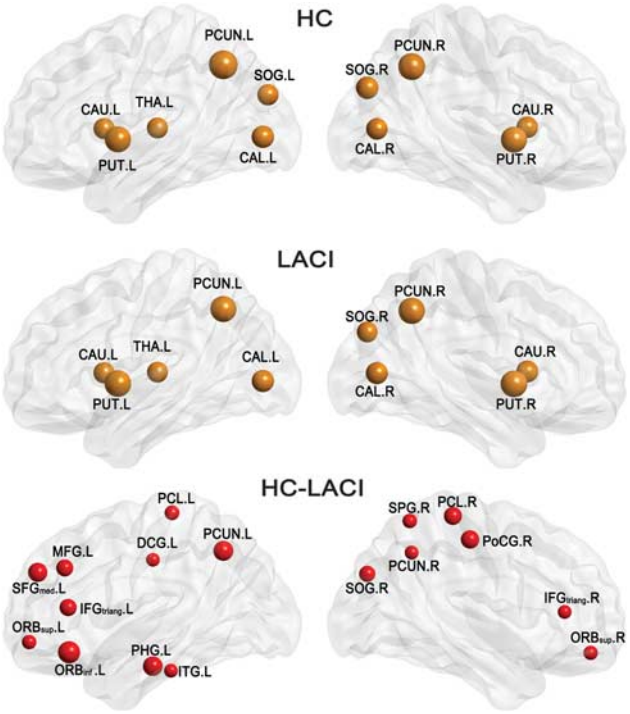

Figure 3. Three-dimensional representations of the hub distributions in the control and LACI groups and the distributions of brain regions with significant group differences in the nodal efficiency at $q < 0.05$ (false discovery rate corrected). The hub nodes are shown in orange, with node sizes representing their nodal efficiency values. The nodes with significant group difference are shown in red, with node sizes indicating the *T* value. The regions with significant group differences mainly localize in the association cortex and the paralimbic system. The regions were mapped onto the cortical surface with an axial view, using the BrainNet Viewer package (http://www.nitrc.org/projects/bnv). CAL, calcarine; CAU, caudate; DCG, median cingulate and paracingulate gyri; HC, healthy control; IFG_{triang}, triangular part of the inferior frontal gyrus; ITG, inferior temporal gyrus; LACI, silent lacunar infarcts; MFG, middle frontal gyrus; ORB_{inf}, orbital part of inferior frontal gyrus; ORB_{sup}, orbital part of the superior frontal gyrus; ORB_{supmed}, medial orbital portions of superior frontal gyrus; PCL, paracentral lobule; PCUN, precuneus; PHG, parahippocampal gyrus; PoCG, postcentral gyrus; SFG_{med}, medial superior frontal gyrus; SOG, superior occipital gyrus; SPG, superior parietal gyrus.

Reproducibility

Among the comparisons of the 100 samplings of split-half subgroups, 75/88 subgroup pairs exhibited significant differences in local and global efficiency. The correlation coefficient of the resultant *t*-scores from group comparisons between each subgroup and the whole group was calculated. The correlation coefficients ranged from 0.60 to 0.80.

The results using DTI studio also showed significant group differences in global efficiency ($P = 0.02$) and local efficiency ($P < 0.001$), which was highly consistent with the earlier findings from our DTI platform. This consistency suggests a high compatibility of our current results across DTI processing platforms (Supplementary Figure 2).

DISCUSSION

Although the LACI group lacked clinical stroke-like symptoms, these patients exhibited poorer performance than HCs on tests of general mental status, memory, attention, executive function, and language ability. Using a DTI neuroimaging technique and a graph theory approach, we demonstrated disruption of WM networks in the LACI group. The main findings are as follows: (1) The structural brain networks of patients with LACI and those of normal controls both exhibit small-world topology; however, the organization of the whole-brain WM network in the patient group was significantly disrupted, as was indicated by reduced global and local efficiencies. (2) A reduction in nodal efficiency was observed in the patient group in multiple brain regions, which were located primarily in the frontal and parietal lobes and the limbic system. (3) Group differences were revealed in the nodal efficiency–behavior correlation analyses in multiple brain regions with multiple cognitive measures, including memory (AVLT-T), attention and executive function (SDMT and SCWT-A-Time), and verbal fluency (Category Verbal Fluency Test). These findings provide us with network-level insights into the neurophysiologic mechanisms that are involved in the abnormality of cognitive patterns in patients with silent brain infarcts in the basal ganglia territory from a network perspective. Our former study found that LACI group exhibited functional connectivity loss, which were associated with cognitive performance.[30] Here, we extended this former study by identifying the disruption of large-scale structural connectivity in LACI and its relationship with cognitive decline.

Table 3. Group differences in correlations between nodal efficiencies of brain regions and cognitive performances

Brain regions	*Cognitive measures*	*Group differences in correlation*	
		$F_{(1,50)}$	P-*value*
IFG_{triang}.L	AVLT-T	6.39	0.015
SFG_{med}.L	CDT	5.80	0.020
PCL.L	CDT	5.54	0.023
PCL.L	ROCF-Copy	6.06	0.017
PCL.R	SCWT-A-Time	4.75	0.034
PCL.R	AVLT-delay recall	4.79	0.033
PCL.R	AVLT-T	8.26	0.006
PCL.R	SDMT	5.51	0.023
PCL.R	CVFT	5.11	0.028
PHG.L	CDT	4.08	0.049
ITG.L	SCWT-A-Time	5.94	0.018

Abbreviations: AVLT, Auditory Verbal Learning Test; CDT, Clock-Drawing Test; CVFT, Category Verbal Fluency Test; HC, healthy control; IFG_{triang}, triangular part of the inferior frontal gyrus; ITG, inferior temporal gyrus; LACI, silent lacunar infarcts; PCL, paracentral lobule; PHG, parahippocampal gyrus; ROCF, Rey-Osterrieth Complex Figure test; SCWT, Stroop Color and Word Test; SDMT, Symbol Digit Modalities Test; SFG_{med}, medial superior frontal gyrus. Differences between LACI and HC in correlation between nodal efficiency and cognitive measures were identified using the general linear model. Eleven correlations showed significant differences between the groups ($P < 0.05$).

The fact that the LACI showed cognitive impairments in our present study is consistent with a previous study, which showed subcortical brain lacunar infarcts can lead to cognitive declines in multiple cognitive functions.[2] It seems to support the motion that brain is a complicated connected system and any light brain lesions may cause comprehensive cognitive consequences.

Disrupted Network Topological Structure in the Silent Lacunar Infarcts

Our results showed that the structural brain networks of both patients with LACI and normal controls have a small-world topology. These results differ from a previous study, which suggested that small-world topology was disrupted in stroke patients.[8] The differences in our findings may be because LACI lesions are not as severe as the lesions in stroke patients. Although the WM networks of patients with LACI showed prominent small-world attributes, the global and local efficiencies were significantly

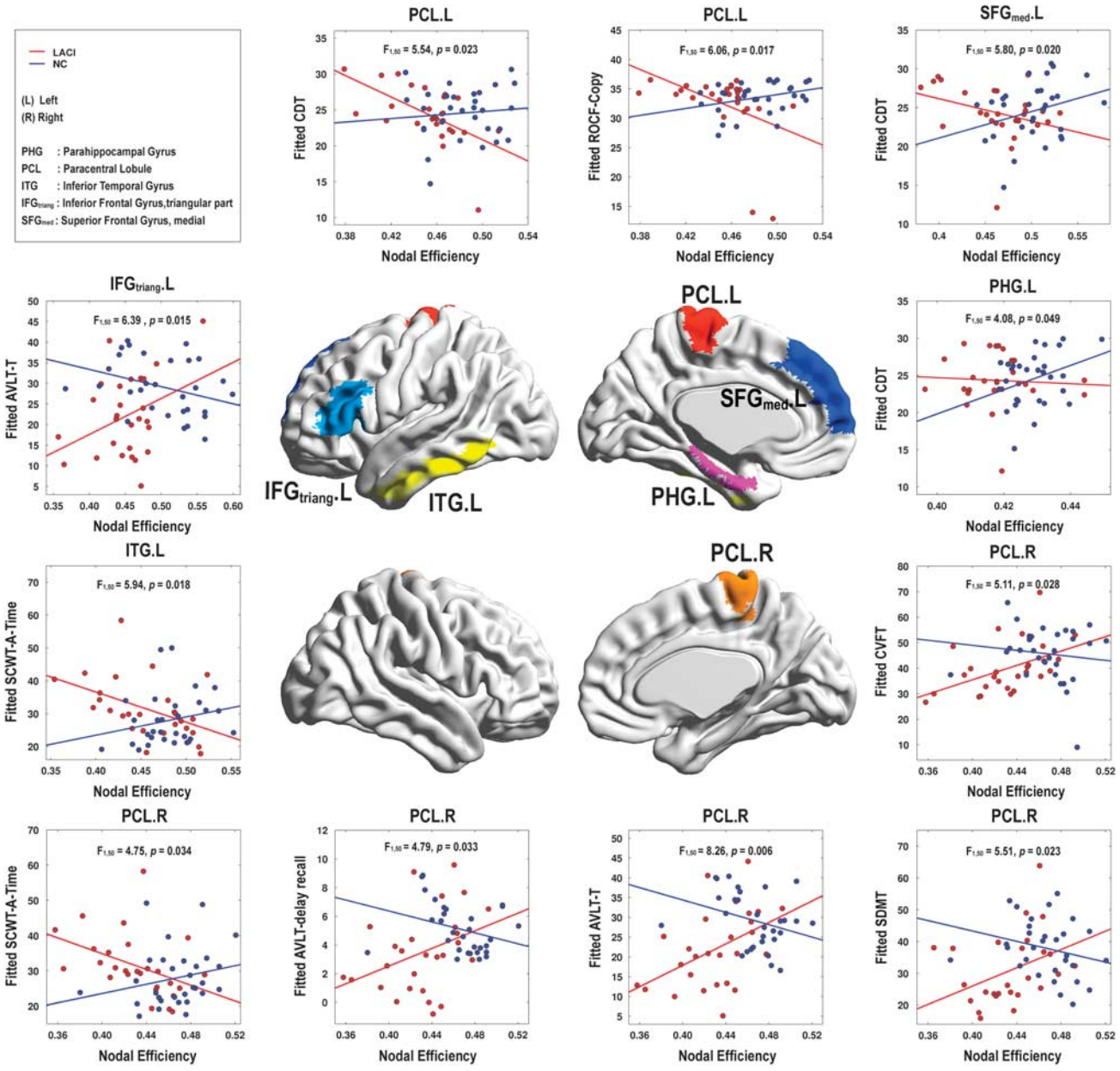

Figure 4. Group difference in correlations between nodal efficiencies and cognitive performances. Among 18 regions showing significant group differences in nodal efficiencies, 6 regions—SFG_{med}.L (dark blue), PCL.L (red), PCL.R (orange), ITG.L (yellow), IFG_{triang}.L (light blue), and PHG.L (violet)—were found to show significant group effects on the correlations between nodal efficiencies and the behavioral scores. IFG_{triang}, triangular part of the inferior frontal gyrus; ITG, inferior temporal gyrus; PCL, paracentral lobule; PHG, parahippocampal gyrus; SFG_{med}, medial superior frontal gyrus.

disrupted in the LACI group. Reduced global and local efficiencies in the LACI group indicated that brain infarcts in the basal ganglia territory could lead to a re-organization of the whole-brain white matter network. Previous studies have demonstrated that cortical brain infarcts can lead to cortical WM network remodeling.[31] However, it is unclear whether disruption of cortical WM networks occurred in patients with subcortical silent brain infarcts. In this report, specific attention was directed toward the disruption of cortical WM networks in patients with brain infarcts located in the basal ganglia. To the best of our knowledge, our study shows for the first time that, as we hypothesized, the WM network was damaged in patients with subcortical silent infarcts compared with normal controls. Our results are consistent with previous studies that suggested that the basal ganglia are anatomically connected with nearly the entire cerebral cortex through basal ganglia–cortical loops.[32] Hence, a small lesion in the basal ganglia can lead to a whole-brain cortical network change through its abundant connections with cortical regions. We further explored the ability of each of the indices or combination of multiple indices to predict changes in brain function (see Supplementary Figure 3). Both ROC analysis and the bootstrap resampling procedure indicated that the global metrics values could be potential biomarkers for the diagnosis of LACI patients. After combining the network indices, we indeed showed improved classification ability for LACI patients.

In addition to global properties, nodal efficiency was also found to be reduced in the LACI group. The SOG.L was a hub node in the HC group but not in the LACI group. Group comparison of the nodes in the whole brain revealed reduced nodal efficiency in the LACI group in multiple brain regions over the entire brain,

primarily located in the orbital and dorsal lateral prefrontal lobe, the parietal lobe, and the limbic system. Previous studies suggested that the majority of the functionally segregated regions of the cerebral cortex provide topographically organized input to the principal input nuclei of the basal ganglia.[32] These cortical regions include the medial and orbital prefrontal cortex (PFC), the dorsal lateral PFC, the premotor and motor cortices, the sensorimotor cortex and the parietal cortex. The regions showing differences in nodal efficiency largely overlap with these cortical regions connecting with the basal ganglia. Several cortex–basal ganglia loops have been reported, such as the two motor circuits[32] and the three non-motor circuits. One of the three non-motor circuits is the dorsal PFC-BG circuit, which has a role in executive function, planning, and working memory.[33] Another non-motor circuit is the orbital PFC-BG circuit, with a role in mediating empathetic and socially appropriate responses. The final non-motor circuit is the anterior cingulate gyrus-BG circuit, which has a role in movement initiation. We hypothesize that differences in nodal efficiency in these regions could be because of damage to the basal ganglia, potentially inducing changes in these circuits and gradually resulting in the abnormality of these cortical regions.

Relationship Between Network Properties and Cognitive Measures

Correlation analyses between network properties and cognitive measures further enhanced our understanding of the neural integration mechanisms that underlie multiple cognitive abilities in both the patient and control groups. Below, we discussed the group differences with regard to nodal efficiency/behavior correlations.

First, the patient group exhibited a negative correlation between the nodal efficiency in the left ITG and one attention/executive function measure (SCWT-A-Time); however, the sign of the correlation was opposite in the controls. The ITG is one of the regions of the ventral stream of visual processing and is believed to be associated with the representation of complex object features.[34] The negative correlation between nodal efficiency in ITG with SCWT-A-Time in the patient group may suggest a shift in the role of ITG toward high-level attention/executive function from basic visual processing to compensate for the cognitive decline caused by brain infarcts in the basal ganglia. The decline in the executive function in the patient group is also reflected in the different nodal efficiency/cognitive measure (i.e., CDT) correlation in the left medial SFG. The control group showed a positive correlation with the CDT in the left medial SFG, whereas the patient group showed the opposite pattern. The left medial SFG has been suggested to be involved in executive mechanisms.[16] Thus, the positive correlation in the control group further supports the notion that this region is involved in the control and monitoring procedure of the clock drawing test, whereas this function might be different in the patient group.

Second, the patient group exhibited positive correlations between nodal efficiency in the right PCL and memory (AVLT-T and AVLT-delay recall) and attention functions (SDMT and SCWT-A-Time), suggesting that this region may be involved in episodic memory and attention in the patient group. However, this region, often referred to as the supplementary motor area, is traditionally believed to be a region of motor planning.[35] This correlation of nodal efficiency in the right PCL with these two measures in the LACI group may also suggest a shift in the role of the PCL from motor functions toward memory and attention functions to compensate for losses in the memory and attention domain. In addition, the patient group also showed a positive correlation between nodal efficiency in the right PCL and verbal fluency (Category Verbal Fluency Test). The left PCL (supplementary motor area) has been suggested to be involved in the coordination of verbal articulation movement during speech production.[36] The positive correlation of nodal efficiency in the right PCL with verbal fluency in the patient group may reflect that the patients use the right homologous region to help improve verbal fluency.

Third, the patient group also showed a positive correlation between the nodal efficiency of the triangular part of the left IFG and one memory measure (AVLT-T); however, the controls showed an opposite correlation pattern. The triangular part of the IFG has been shown to have a role in the cognitive control of memory.[37] The positive correlation between this region and the memory measure (AVLT-T) may suggest that the patient group expends more effort (more cognitive control) for tasks involving memory retrieval.

Last, the control group showed a positive correlation between nodal efficiency in the left PHG with one spatial processing measure (CDT), whereas the patient group barely showed a correlation. The PHG is an important region involved in memory encoding and retrieval, especially in visuospatial memory encoding and retrieval.[38] The positive correlation between nodal efficiency in this region with the spatial processing measure (CDT) in the control but not in the patient group suggests that the function of this region in visuospatial memory might be impaired in the patients. Meanwhile, the control group also showed positive correlations with two spatial processing measures (CDT and ROCF-copy) in the left PCL, whereas the patient group showed an opposite pattern. As mentioned above, the left PCL is usually considered to be involved in motor coordination, and the positive correlation in the control group suggests that this region may be involved in the motor coordination required for the completion of these two tests, whereas the opposite pattern in the patient group suggests different function in this region.

In summary, our findings suggest that the relationship between nodal efficiency and multiple cognitive measures is different in the patient group because of infarcts in the basal ganglia. These findings suggest that the presence of brain infarcts in the basal ganglia can profoundly change brain organization and that network properties can provide important explanations for the individual differences in multiple cognitive functions and for the cognitive decline in the patient group.

CONCLUSION

In conclusion, this study revealed global and local topological disruption in basal ganglia-related cortical WM networks in the LACI group. In addition, network properties in the patient group were determined to be associated with cognitive decline in multiple domains. These findings provided a new explanation for the cognitive dysfunction in the LACI that subcortical lacunar infarcts in the basal ganglia may affect neuropsychological performance through the disruption of cortical structural network. The basal ganglia are anatomically connected with cortical areas by multiple subcortical–cortical circuits. Our findings further indicated that even small brain lesions in subcortical brain regions may cause extensive cognitive dysfunction because of the abundant subcortical–cortical anatomic connections.

Close connection has been observed between subcortical silent lacunar infarcts and the risk of subsequent stroke and dementia. Thus, our findings highlight the need for more medical attention and care for individuals with this disease. Specifically, our finding highlighted the necessity to identify and evaluate the clinical outcome by combining neuroimaging screening with neuropsychological tests in old population. In addition, in this study, we identified some specific nodes and hubs, which were affected in the LACI group. These regions may represent the susceptible regions to silent brain infarcts that can be candidates as potential neuroimaging markers of intervention to guide future clinical practice.

Limitations

Despite interesting findings in the present study, a few limitations need to be addressed. First, DTI-deterministic tractography

method was utilized to reconstruct human WM networks in this study. Despite being widely used, this method has a limited capacity for resolving fiber crossing. New diffusion tractography methods being able to handle crossing fibers shall be considered to explore the LACI brain topological properties of WM networks in the future.[39,40] Second, because the current study is only cross-sectional, it is hard to reveal the gradually remodeling process of the basal ganglia-related WM network in the LACI. Longitudinal data shall be used to investigate this issue in the future. Third, because of relatively limited number of subjects in the current study, there was not enough power to investigate the white matter network changes related to the lesion size and location of subcortical infarcts, which shall be investigated in the future. Finally, the imaging sample used in the current study was not selected by strict random sampling method from the entire study participant group (and definitely not from the entire population), the relatively high percentage of the LACI patients in our imaging subgroup is not reflective of the general population.

AUTHOR CONTRIBUTIONS

JT, SZ, and YC analyzed the data and drafted the manuscript; YC and JZ recruited the study population and conducted the neuropsychological tests; KC and AF advised on biostatistical methodology and revised manuscript for important intellectual content; JZ, YH, and GG assisted with analysis of the data and manuscript revision for important intellectual content; ZZ conceived the original idea for the study, supervised in the conception, and revised the manuscript. All the authors read and approved the final manuscript.

DISCLOSURE/CONFLICT OF INTEREST

The authors declare no conflict of interest.

ACKNOWLEDGMENTS

The authors thank all the volunteers and patients for their participation in the study and anonymous reviewers for their insightful comments and suggestions. The authors also thank Jennifer Wu from the MIT Math department for her assistance.

REFERENCES

1 Vermeer SE, Longstreth WT, Koudstaal PJ. Silent brain infarcts: a systematic review. *Lancet Neurol* 2007; **6**: 611–619.
2 Arvanitakis Z, Leurgans SE, Barnes LL, Bennett DA, Schneider JA. Microinfarct pathology, dementia, and cognitive systems. *Stroke* 2011; **42**: 722–727.
3 Heringa SM, Reijmer YD, Leemans A, Koek HL, Kappelle LJ, Biessels GJ. Multiple microbleeds are related to cerebral network disruptions in patients with early Alzheimer's disease. *J Alzheimers Dis* 2014; **38**: 211–221.
4 Reijmer YD, Freeze WM, Leemans A, Biessels GJ. The effect of lacunar infarcts on white matter tract integrity. *Stroke* 2013; **44**: 2019–2021.
5 Reijmer YD, Fotiadis P, Martinez-Ramirez S, Salat DH, Schultz A, Shoamanesh A *et al.* Structural network alterations and neurological dysfunction in cerebral amyloid angiopathy. *Brain* 2015; **138**: 179–188.
6 Sporns O, Tononi G, Kotter R. The human connectome: a structural description of the human brain. *PLoS Comput Biol* 2005; **1**: e42.
7 Sporns O. Structure and function of complex brain networks. *Dialogues Clin Neurosci* 2013; **15**: 247–262.
8 Wang L, Yu C, Chen H, Qin W, He Y, Fan F *et al.* Dynamic functional reorganization of the motor execution network after stroke. *Brain* 2010; **133**(Pt 4): 1224–1238.
9 Shu N, Liang Y, Li H, Zhang J, Li X, Wang L *et al.* Disrupted topological organization in white matter structural networks in amnestic mild cognitive impairment: relationship to subtype. *Radiology* 2012; **265**: 518–527.
10 Yao Z, Zhang Y, Lin L, Zhou Y, Xu C, Jiang T. Abnormal cortical networks in mild cognitive impairment and Alzheimer's disease. *PLoS Comput Biol* 2010; **6**: e1001006.
11 Lo CY, Wang PN, Chou KH, Wang J, He Y, Lin CP. Diffusion tensor tractography reveals abnormal topological organization in structural cortical networks in Alzheimer's disease. *J Neurosci* 2010; **30**: 16876–16885.
12 Supekar K, Menon V, Rubin D, Musen M, Greicius MD. Network analysis of intrinsic functional brain connectivity in Alzheimer's disease. *PLoS Comput Biol* 2008; **4**: e1000100.
13 Reijmer YD, Leemans A, Caeyenberghs K, Heringa SM, Koek HL, Biessels GJ. Disruption of cerebral networks and cognitive impairment in Alzheimer disease. *Neurology* 2013; **80**: 1370–1377.
14 Bellebaum C, Koch B, Schwarz M, Daum I. Focal basal ganglia lesions are associated with impairments in reward-based reversal learning. *Brain* 2008; **131**: 829–841.
15 Mayor-Dubois C, Maeder P, Zesiger P, Roulet-Perez E. Visuo-motor and cognitive procedural learning in children with basal ganglia pathology. *Neuropsychologia* 2010; **48**: 2009–2017.
16 Talati A, Hirsch J. Functional specialization within the medial frontal gyrus for perceptual go/no-go decisions based on "what," "when," and "where" related information: an fMRI study. *J Cogn Neurosci* 2005; **17**: 981–993.
17 Wardlaw JM, Smith EE, Biessels GJ, Cordonnier C, Fazekas F, Frayne R *et al.* Neuroimaging standards for research into small vessel disease and its contribution to ageing and neurodegeneration. *Lancet Neurol* 2013; **12**: 822–838.
18 Fisher CM. Lacunes: Small, deep cerebral infarcts. *Neurology* 2011; **77**: 2104.
19 Wang L, Li H, Liang Y, Zhang J, Li X, Shu N *et al.* Amnestic mild cognitive impairment: topological reorganization of the default-mode network. *Radiology* 2013; **268**: 501–514.
20 Cui Z, Zhong S, Xu P, He Y, Gong G. PANDA: a pipeline toolbox for analyzing brain diffusion images. *Front Hum Neurosci* 2013; **7**: 42.
21 Leemans A, Jones DK. The B matrix must be rotated when correcting for subject motion in DTI data. *Magn Reson Med* 2009; **61**: 1336–1349.
22 Ashburner J, Friston KJ. Unified segmentation. *Neuroimage* 2005; **26**: 839–851.
23 Mori S, Crain BJ, Chacko V, Van Zijl P. Three dimensional tracking of axonal projections in the brain by magnetic resonance imaging. *Ann Neurol* 1999; **45**: 265–269.
24 Gong G, Rosa-Neto P, Carbonell F, Chen ZJ, He Y, Evans AC. Age-and gender-related differences in the cortical anatomical network. *J Neurosci* 2009; **29**: 15684–15693.
25 Achard S, Bullmore E. Efficiency and cost of economical brain functional networks. *PLoS Comput Biol* 2007; **3**: e17.
26 Latora V, Marchiori M. Efficient behavior of small-world networks. *Phys Rev Lett* 2001; **87**: 198701.
27 Watts DJ, Strogatz SH. Collective dynamics of 'small-world'networks. *Nature* 1998; **393**: 440–442.
28 Maslov S, Sneppen K. Specificity and stability in topology of protein networks. *Science* 2002; **296**: 910–913.
29 Yan C, Gong G, Wang J, Wang D, Liu D, Zhu C *et al.* Sex-and brain size–related small-world structural cortical networks in young adults: a DTI tractography study. *Cereb Cortex* 2011; **21**: 449–458.
30 Chen Y, Wang J, Zhang J, Zhang T, Chen K, Fleisher A *et al.* Aberrant functional networks connectivity and structural atrophy in silent lacunar infarcts: relationship with cognitive impairments. *J Alzheimers Dis* 2014; **42**: 841–850.
31 van Meer MPA, Otte WM, van der Marel K, Nijboer CH, Kavelaars A, van der Sprenkel JWB *et al.* Extent of bilateral neuronal network reorganization and functional recovery in relation to stroke severity. *J Neurosci* 2012; **32**: 4495–4507.
32 Smith Y, Bevan M, Shink E, Bolam J. Microcircuitry of the direct and indirect pathways of the basal ganglia. *Neuroscience* 1998; **86**: 353.
33 McNab F, Klingberg T. Prefrontal cortex and basal ganglia control access to working memory. *Nat Neurosci* 2007; **11**: 103–107.
34 Denys K, Vanduffel W, Fize D, Nelissen K, Peuskens H, Van Essen D *et al.* The processing of visual shape in the cerebral cortex of human and nonhuman primates: a functional magnetic resonance imaging study. *J Neurosci* 2004; **24**: 2551–2565.
35 Lee D, Quessy S. Activity in the supplementary motor area related to learning and performance during a sequential visuomotor task. *J Neurophysiol* 2003; **89**: 1039–1056.
36 Saarinen T, Laaksonen H, Parviainen T, Salmelin R. Motor cortex dynamics in visuomotor production of speech and non-speech mouth movements. *Cereb Cortex* 2006; **16**: 212–222.
37 Badre D, Wagner AD. Left ventrolateral prefrontal cortex and the cognitive control of memory. *Neuropsychologia* 2007; **45**: 2883–2901.
38 Epstein R, Kanwisher N. A cortical representation of the local visual environment. *Nature* 1998; **392**: 598–601.
39 Jones DK, Knösche TR, Turner R. White matter integrity, fiber count, and other fallacies: the do's and don'ts of diffusion MRI. *Neuroimage* 2013; **73**: 239–254.
40 Tournier J-D, Mori S, Leemans A. Diffusion tensor imaging and beyond. *Magn Reson Med* 2011; **65**: 1532–1556.

Supplementary Information accompanies the paper on the Journal of Cerebral Blood Flow & Metabolism website (http://www.nature.com/jcbfm)